Rational design of disulfide bonds to increase thermostability of Rhodococcus opacus catechol 1,2 dioxygenase

Lister, Joshua G. R.; Loewen, Matthew E.; Loewen, Michele C.; St-Jacques, Antony D.

Publisher's version / Version de l'éditeur:
https://doi.org/10.1002/bit.28808
Biotechnology and Bioengineering, 2024-08-01

Received: 12 April 2024 | Revised: 25 June 2024 | Accepted: 7 July 2024

DOI: 10.1002/bit.28808

ARTICLE

BIOTECHNOLOGY AND BIOENGINEERING WILEY

Rational design of disulfide bonds to increase thermostability of *Rhodococcus opacus* catechol 1,2 dioxygenase

Joshua G. R. Lister[1] | Matthew E. Loewen[2] | Michele C. Loewen[1,3] | Antony D. St-Jacques[3]

[1]Department of Chemistry and Biomolecular Sciences, University of Ottawa, Ottawa, Ontario, Canada

[2]Department of Veterinary Biomedical Sciences, University of Saskatchewan, Saskatoon, Saskatchewan, Canada

[3]National Research Council of Canada, Aquatic and Crop Resources Development, Ottawa, Ontario, Canada

Correspondence
Michele C. Loewen, Department of Chemistry and Biomolecular Sciences, University of Ottawa, Ottawa, ON, Canada.
Email: michele.loewen@nrc-cnrc.gc.ca

Funding information
National Research Council of Canada; Natural Sciences and Engineering Research Council of Canada

Abstract

Catechol 1,2 dioxygenase is a versatile enzyme with several potential applications. However, due to its low thermostability, its industrial potential is not being met. In this study, the thermostability of a mesophilic catechol 1,2 dioxygenase from the species *Rhodococcus opacus* was enhanced via the introduction of disulphide bonds into its structure. Engineered designs (56) were obtained using computational prediction applications, with a set of hypothesized selection criteria narrowing the list to 9. Following recombinant production and purification, several of the designs demonstrated substantially improved protein thermostability. Notably, variant K96C-D278C yielded improvements including a 4.6°C increase in T_{50}, a 725% increase in half-life, a 5.5°C increase in T_m, and a >10-fold increase in total turnover number compared to wild type. Stacking of best designs was not productive. Overall, current state-of-the-art prediction algorithms were effective for design of disulfide-thermostabilized catechol 1,2 dioxygenase.

KEYWORDS
catechol dioxygenase, disulfide bond, protein engineering, *Rhodococcus opacus*, thermostabilization

1 | INTRODUCTION

In proteins, disulfide cross-links are formed by the oxidation of two cysteines (Landeta et al., 2018; Zhang et al., 2011). Previous studies have shown that such disulfide linkages play crucial roles in the thermostabilization, recognition and activation of proteins (Karimi et al., 2016; Roesler & Rao, 2000). Disulfide linkages serve to improve the thermostability of proteins by influencing the thermodynamics of protein folding. These linkages stabilize the native, folded form of a protein by lowering the entropy of the unfolded form, thus destabilizing it and driving the folding-unfolding equilibrium towards the folded form (Abkevich & Shakhnovich, 2000; Hogg, 2003). Based on this functionality, many studies have sought to utilize engineered disulfide bonds to increase the thermostability of proteins. As it pertains to enzymes, the engineering of disulfide bonds has been repeatedly applied, with two very successful examples including the stabilization of alkaline α-amylase(Long

Michele C. Loewen and Antony D. St-Jacques contributed equally.

et al., 2014) and 1,4-β-endoglucanase (Badieyan et al., 2012). At the same time, in recent years several software applications including Yosshi (Suplatov et al., 2019), DbD2 (Craig & Dombkowski, 2013), and SSBondPre (Gao et al., 2020) have been developed that can predict potential residue pairs for the construction of disulfide bonds in a given protein structure. While useful, these computational tools often predict too many putative disulphide bond locations to test experimentally. Thus, it has been suggested that additional criteria are needed to limit the number of locations for testing (Kazlauskas, 2018).

The focus of this current engineering study is the enzyme catechol 1,2 dioxygenase from the species *Rhodococcus opacus* (*Rho*1,2-CTD) (Matera et al., 2010). It is a type of intradiol (also known as endo-diol) dioxygenase that belongs to a larger family of ring-cleaving dioxygenases, utilized by various microorganisms in the metabolism of aromatic compounds (Bugg & Lin, 2001). Intradiol dioxygenases employ nonheme Fe(III) to cleave catechol and related aromatic compounds in between the hydroxyl substituents (and not external to them) via the incorporation of two atoms of molecular oxygen (Figure 1) (Bugg & Lin, 2001; Bugg & Ramaswamy, 2008; Que & Ho, 1996). The nonheme Fe(III) is coordinated by two tyrosine's (Tyr 162 and Tyr196), two histidine's (His 220 and His 222), and a water or hydroxide ion (Supporting Information S1: Figure S1) (Matera et al., 2010).

The cleavage product of catechol arising from application of *Rho*1,2-CTD is *cis*,*cis*-muconic acid (ccMA). The ccMA molecule is a high-value bio-product with potential applications in the manufacture of emerging performance-enhanced materials such as functional resins, plastics, agrochemicals, and pharmaceuticals (Rorrer et al., 2016; N.-Z. Xie, Liang, et al., 2014). Current production methods for many of these products are unsustainable (Environment and Climate Change Canada, 2023; Thiemens & Trogler, 1991). As such, development of a single enzyme-based conversion of catechol into ccMA could provide a superior production strategy with impact across many industrial fields. However, it has been shown that *Rho*1,2-CTD loses 55% and 90% activity upon heating to its optimal reaction temperature for 1 and 4 h, respectively (Shumkova et al., 2009), decreasing economic viability. The discovery of new more stable catechol dioxygenases or improvement of the thermostability of existing catechol dioxygenases by state-of-the-art protein engineering strategies is essential.

Here, we report enhancement of the thermostability of *Rho*1,2-CTD via the rational design and engineering of disulfide bonds into its structure. Designs were developed using computational software applications to predict potential residue pairs for disulfide bond engineering. The obtained list of designs (56 total) was reduced to a more easily testable number (9) by the application of a set of hypothesized selection criteria. Functional characterization of the 9 selected designs yielded a range of activities, including significantly improved protein thermostability, with a minimal loss in catalytic activity. That current state-of-the-art disulfide bond prediction

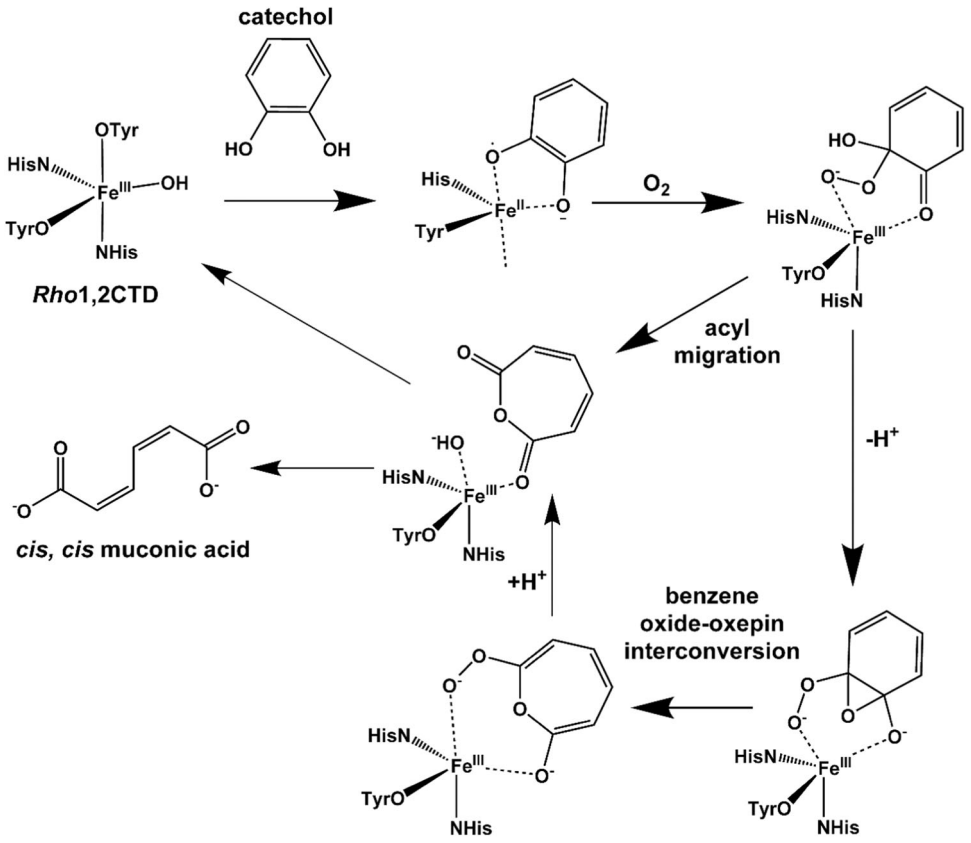

FIGURE 1 Scheme of proposed catechol 1,2-dioxygenase catalytic mechanism displaying the 2 proposed mechanisms for the degradation of catechol (T. D. H. Bugg & Lin, 2001; T. D. Bugg & Ramaswamy, 2008; Que & Ho, 1996).

algorithms can be highly effective for designing improved protein thermostability into biocatalysts is highlighted. At the same time, the potential to stabilize members of the intradiol ring-cleaving family of enzymes is emphasized.

2 | MATERIALS AND METHODS

2.1 | Chemicals

All chemicals were purchased from Millipore-Sigma unless otherwise stated below.

2.2 | Computational design strategy

Sequence and structural data for *Rho*1,2-CTD (NCBI accession code: WLF46330, PDB ID: 3HHY)(Matera et al., 2010) were fed into 3 disulfide bond prediction software applications; Yosshi (Suplatov et al., 2019), SSBondPre (Gao et al., 2020), and DisulfideByDesign2 (Craig & Dombkowski, 2013) to generate potential disulfide bond locations using default settings. A set of hypothesized selection criteria was applied to the list to subsequently narrow it down to a practical testable number of bonds (Supporting Information S1: Figure S2). In short, disulfide bonds were eliminated if: i) residues forming the bond were less than 10 residues apart in the primary structure, ii) if the putative bond was within 5 Å of any atom making up any active site amino acids (backbone and side chain; atoms from Tyr162, Tyr196, His220, His222) as well as the Fe(III), or catechol substrate, iii) if residues forming the bond were part of the 25% least flexible residues (as determined by b-factors), or iv) if mutations were predicted to be strongly destabilizing (as determined by program DynaMut2 (Rodrigues et al., 2021)). The basis of the criterion concerning b-factors was two former studies that showed stabilizing disulfide mutations are most often found in regions of medium to high mobility (Dani et al., 2003; Matsumura et al., 1989). Mobile residues are likely the first to undergo conformational changes towards unfolded forms. Thus, we reasoned that decreasing the entropy of these mobile regions will destabilize these partially unfolded intermediates more than decreasing the entropy of less mobile regions that are likely unchanged between the folded and intermediate unfolded state. One exception was made regarding the b-factors criterion for H85C-A252C because it was predicted by DynaMut2 to be strongly stabilizing. b-factors were obtained from PDB ID: 3HGI using PyMOL (PyMOL, 2024).

2.3 | Cloning and recombinant expression of *Rho*1,2-CTD and variants

Cloning of *Rho*1,2-CTD was described previously (Forero et al., 2023). cDNAs encoding the variants, were generated by GenScript Inc (Piscataway) by direct mutagenesis of the pET31b + -*Rho*1,2-CTD expression vector and confirmation by DNA sequencing. The double disulfide mutants were also generated by GenScript Inc, where the single disulphide encoding *Rho*1,2-CTD K96C-D278C variant expression vector was used as the template and site changes made to add A35C-Q211C and H85C-A252C to this respectively. Starter cultures were generated by inoculating a small volume of Lysogeny-Broth (LB) media (10 g Tryptone, 10 g NaCl, 5 g Yeast Extract per 1 L) containing 100 µg/mL ampicillin with *E. coli* BL21(DE3) cells transformed with a pET31b+ vector (Novagen/EMD Millipore) encoding codon optimized *Rho*1,2-CTD (NCBI accession code: WLF46330). The coding region was synthesized by GenScript, and sub-cloned into the NdeI and XhoI restriction sites of the pET31b+ vector, without a stop codon to include a C-terminal His-tag. Starter cultures were grown overnight at 37°C with shaking at 275 rpm. Enzyme expression was achieved by inoculating (1:100) larger cultures of LB medium containing 100 µg/mL ampicillin with the starter culture. The cultures were grown at 37°C at 275 rpm until an OD_{600} of 0.3–0.4 was achieved, at which point the temperature was turned down to 18°C and cultures were further grown to an OD_{600} of 0.6–0.7. Expression was induced with 0.7 mM of isopropyl ß-D-1-thiogalactopyranoside (IPTG) and cultures were shaken at 18°C for 18-24 h at 150 rpm. Cells were harvested by centrifugation at 3250 x *g* for 30 min at 4°C. Pellets were stored at −20°C. Coding DNA sequences for each of the *Rho*1,2-CTD disulphide designs were generated by site-directed mutagenesis and subcloned into the pET31b+ vector and treated as described above.

2.4 | Recombinant Rho1,2-CTD purification

Cell pellets were thawed for 15 min on ice and resuspended in Lysis buffer (10 mM Tris-HCl, 150 mM NaCl, 10 mM imidazole, 2 mM $MgCl_2$, 5 mM dithiothreitol, 1 mM phenylmethanesulfonyl (PMSF; protease inhibitor), 3 U/mL benzonase, 0.5 mg/mL lysozyme, adjusted to pH 8.0). Cells were lysed using a French Press. Lysate was centrifuged at 17,000 x *g* for 30 min at 4°C. *Rho*1,2-CTD was then purified by immobilized metal affinity chromatography using a Bio-Rad column and Ni-NTA (Qiagen) resin. Ni-NTA slurry was added to a 25 mL Bio-Rad column and the column was equilibrated with 10 column volumes of lysis buffer. Supernatant from the cell lysate preparation was added to the column and the flowthrough was collected. The column was then washed with 1 column volume of wash buffer (10 mM Tris-HCl, 150 mM NaCl, 20 mM imidazole, adjusted to pH 8.0) 3 times and eluates from washes 1-3 collected. The protein was then eluted by adding 1 column volume of elution buffer (10 mM Tris-HCl, 150 mM NaCl, 250 mM imidazole, adjusted to pH 8.0), the column was inverted several times and incubated for 4 min before collecting the elution fraction. This step was repeated twice more. The purified *Rho*1,2-CTD sample from the three elutions was applied to a 120 mL HiLoad™ 16/60 Superdex200 prep grade column (GE Healthcare Life Sciences) pre-equilibrated with gel filtration buffer (10 mM Tris-HCl, 150 mM NaCl, adjusted to pH 8.0) using an AKTA pure 25 L FPLC system (Cytiva) with UNICORN™ 7.0 software, at a flow rate of 0.3 mL/min. Obtained purified recombinant *Rho*1,2CTD was quantified by Bradford assay (Bradford, 1976).

2.5 | *Rho*1,2-CTD Kinetic Activity Assay

Enzyme activity was followed by a continuous assay that detects 3-methyl *cis*,*cis* muconic acid formation over time from 3-methyl catechol hydrolysis at 260 nm as previously described (Matera et al., 2010). The assay was adapted to support a high throughput format in a UV Star 96 well microplate. The 300 µL reaction mixture contained 50 mM Tris pH 7.2. After 15 min of pre-incubation at reaction temperature, the reaction was started by adding the enzyme, and the increase in absorbance at 260 nm ($\varepsilon = 16.0\ mM^{-1} \cdot cm^{-1}$) was monitored in a SpectraMax M5e spectrophotometer. Unless otherwise indicated, enzymatic activity was assayed at 40°C. Initial rates for all the enzymes were determined in triplicate by means of the assay described above using an enzyme concentration of 1.5 µg/mL, with 3-methylcatechol concentrations varying from 2.19 to 70 µM. Rates were fitted to the Michaelis–Menten equation (Michaelis & Menten, 1913) (v = (Vmax[S])/(Km + [S]) using GraphPad Prism version number 9.1.12. Apparent k_{cat} values were calculated on the basis of the molecular mass of the enzyme monomeric polypeptide (31740.73 Da), using the equation kcat = Vmax/[ET], with ET representing total enzyme concentration in mg/mL.

2.6 | Temperature of half-inactivation (T_{50}) assay

T_{50} tests were performed using the kinetic activity assay described above after heat treatment as previously described previously (Xie, An, et al., 2014). Heat treatment of purified protein was carried out by incubating the protein in 0.2 mL PCR tubes in a BioRad T100 thermal cycler. Proteins (30 µL) were tested at previously determined optimal concentration which varied between variants. Optimal concentrations were based on the amount of enzyme that produced an equivalent activity level at 25°C for all variants. This allowed a more reliable analysis in the face of widely differing ranges of activities observed across variants at a single standard concentration. While the possible impact of aggregation differences at different concentrations cannot be ignored, this is true also for variants at the same concentration as well. All proteins were heated at temperatures ranging from 30°C to 55°C at intervals of 5°C for 15 min and cooled at 4°C for 10 min, followed by equilibration at the kinetic assay temperature of 25°C for 5 min. Samples were centrifuged to remove any aggregated protein before assaying the enzymatic activity using a 3-methylcatechol concentration of 65 µM. Activity of enzyme without undergoing heat treatment was considered to be 100%; the residual activities were quantitatively measured after heating at different temperatures for 15 min. The T_{50} value is the temperature at which enzyme activity is reduced to 50% after a 15-min heat treatment. The precise value was obtained by determination of the inflection point of a fit of the residual activities at certain temperatures to a sigmoidal plot (sigmoidal Boltzmann fit using GraphPad Prism version number 9.1.12).

2.7 | Half-Life ($t_{1/2}$) assay

Half-life was determined as described previously (Xie, An, et al., 2014). Each *Rho*1,2-CTD variant (0.2 mg/mL) was incubated using a BioRad T100 thermal cycler at 40°C for time intervals ranging from 15-min to 2-h intervals. Their residual activities were assayed at 40°C with a 3-methylcatechol concentration of 65 µM using the assay described above. The data were fitted to first-order plots and analyzed with the first-order rate constants (k_d) determined by linear regression of ln (residual activity) versus incubation time (t). The time required for the residual activity to be reduced to half ($t_{1/2}$) was calculated using the following equation: $t_{1/2} = \ln 2/k_d$. The 40°C temperature was selected based on this being the optimal temperature for wild type.

2.8 | Thermal shift (T_m) assay

Thermal shift assays were performed as previously described (Niesen et al., 2007) using an iQ5 qPCR machine (BioRad). Enzyme and SYPRO Orange Dye (ThermoFisher) were added to appropriate wells in a Hard-Shell High Profile 96-well Semi-Skirted PCR plate (BioRad) at a final concentration of 400 µg/mL and 5X, respectively in a 50 mM Tris buffer, pH 7.2. The PCR plates were sealed using Microseal "B" seals (BioRad) and placed in the qPCR machine. The assay was performed using the melt curve function of the iQ5 qPCR; with a starting point at 20°C and an endpoint of 95°C. Measurements were taken at 0.5°C intervals for 15 s at each temperature. Melting points were found at the global minimum of the first derivative of RFU as was done previously (Rosa et al., 2015).

2.9 | Verification of disulfide bonds formation

The formation of disulfide bonds in *Rho*1,2-CTD variants was examined using 5,5′-dithiobis-(2-nitrobenzoic acid (DTNB) which can quantitatively measure the number of free sulfhydryl groups in protein structure (Ellman, 1959). Two samples were prepared: a reduced and a non-reduced sample. The reduced sample was prepared by mixing the protein sample with 100 mM DTT, while the non-reduced was mixed with the same volume of reaction buffer (0.1 M sodium phosphate, 1 mM EDTA, pH 8.0). Samples were mixed and incubated at 37°C for two h, and then underwent buffer exchange using Amicon Ultra Centrifugal Filters (Millipore) to remove DTT. Samples were then concentrated and mixed with reaction buffer and 0.2 mM DTNB. Samples were incubated for 15 min at room temperature and absorbance was measured at 412 nm.

3 | RESULTS

3.1 | Disulphide designs generation

Disulfide bond prediction software programs DbD2 (Craig & Dombkowski, 2013), Yosshi (Suplatov et al., 2019), and SSBondPre

(Gao et al., 2020) were used to predict potential locations for the introduction of disulfide bonds. These software applications predicted a total of 56 unique possible disulfides. To reduce this to a number that could be practically tested experimentally, a set of selection criteria were developed to putatively prioritize linkages for triage, although whether any significant hits were eliminated or enriched by this selection was not ultimately tested herein (Supporting Information S1: Figure S2). Nonetheless, 12 residue pairs were eliminated by applying a distance limitation for the two residues in the primary sequence, where they must be at least 10 amino acids apart along the chain in the primary sequence. This limitation was based on the idea that small rings will provide little entropic reduction to the unfolded form (Pace et al., 1988). At the same time, there is also a school of thought that considers pairs that are too close together might produce potential structural conflicts in the native secondary structure (Betz, 1993; Petersen et al., 1999) and destabilize the folded form (Betz, 1993; Petersen et al., 1999) and destabilize the folded form. Subsequently, 14 residue pairs, in which any the two Cα's of the targeted residues were located within 5 Å of essential active site coordinating residues (Tyr162, Tyr196, His220, His222), the Fe(III), or the substrate in the crystal structure PDB ID: 3HHY were eliminated. This limitation was set to ensure preservation of the catalytic centre and its associated activity. Following this, b-factors from crystal structure 3HHY were analyzed showing that 15 of the proposed bonds were made up of residues that were among the most rigid 25% in the protein, which were then were eliminated. Finally, structural and sequence information was analyzed using DynaMut2(Rodrigues et al., 2021), a web server that combines Normal Mode Analysis (NMA) and graph-based signatures to predict the effects of missense mutations on protein stability. From this criterion, 6 residue pairs that were predicted to be destabilizing with a high level of confidence were rejected. This left a total of 9 potential residue pairs, 7 intra-monomer bonds and 2 inter-monomer bonds (Figure 2). Overall, the selection criteria reduced the number of designs to test by 84%. But again, we remind the reader that whether any significant hits were eliminated or enriched goes beyond the

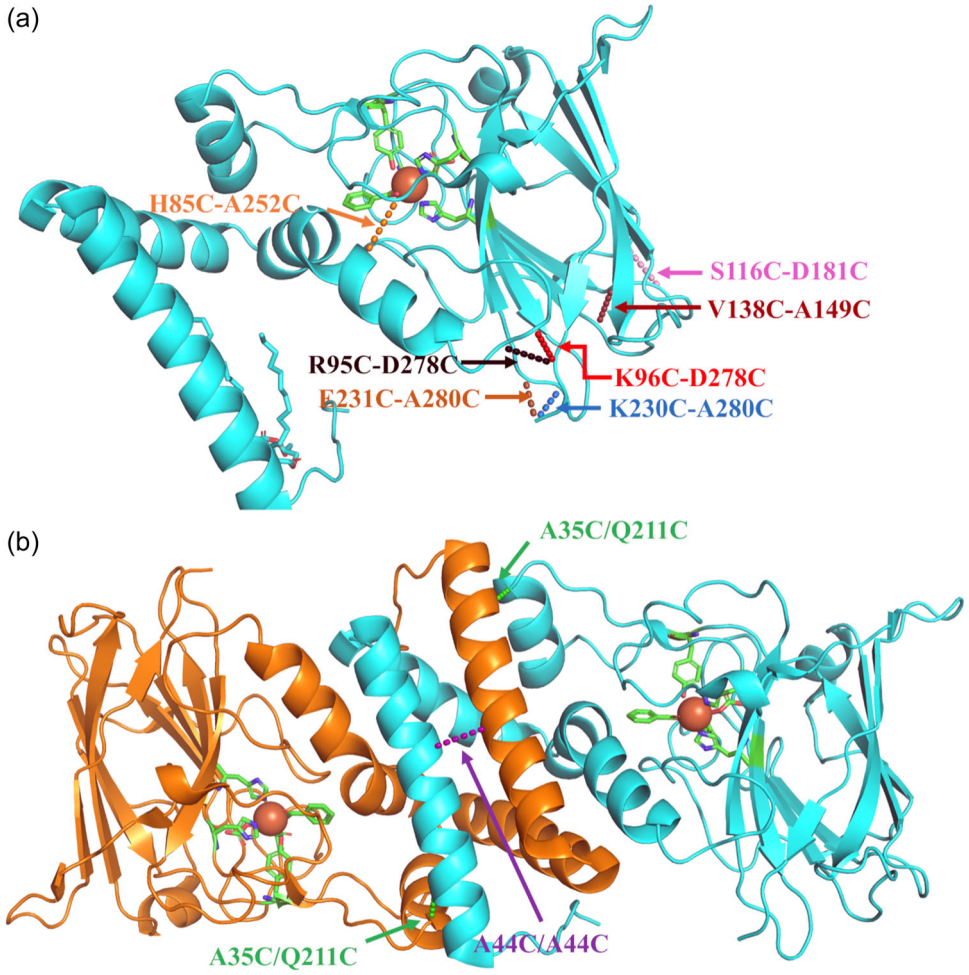

FIGURE 2 Cartoon representation of Rho1,2-CTD crystal structure (PDB ID: 3HGI) showcasing locations of disulfide bonds selected for testing. (a) Single monomeric polypeptide view showcasing locations of intra-monomer bonds. (b) Biological assembly of 2 interacting monomeric units, showcasing locations of inter-monomer bonds. Locations of bonds are showcased by a dashed line connecting two parts of the protein. The double stacked variants included DB1: K96C-D278C + A35C/Q211C and DB2: K96C-D278C + H85C-A252C. The active site residues of the enzyme is highlighted in green and catalytic iron is shown as an orange sphere. Images were produced using PyMol.

scope of this current study, but remains an interesting question for future consideration. In terms of annotation, intra-monomer disulfide bonds are denoted with a dash between the residue pair making up the bond while inter-monomer bonds are denoted with a slash. Following characterization of the single disulphide variants, the top performer was stacked with each of the next two best performers to create two double-disulphide variants (DB1: K96C-D278C + A35C/Q211C and DB2: K96C-D278C + H85C-A252C) to test for possible additive effects.

3.2 | Recombinant generation and purification of wild-type *Rho*1,2-CTD and variants

Coding DNA sequences for each of the *Rho*1,2-CTD disulphide designs were generated by site-directed mutagenesis and subcloned into the pET31b+ vector. Wild type *Rho*1,2-CTD and the disulphide variants were recombinantly expressed in *E. coli* BL21 cells. Enzymes were purified by Ni-NTA metal affinity chromatography (Supporting Information S1: Figure S3), followed by size-exclusion purification (Supporting Information S1: Figure S4), and quantified (Supporting Information S1: Figure S5).

3.3 | Thermostability of *Rho*1,2-CTD and disulphide variants

Protein stability comes in two flavours: i) thermodynamic stability, which is related to low-levels of unfolded and partially-folded states in equilibrium with the native, functional protein, and ii) kinetic stability, which is related to a high free-energy barrier "separating" the native state from the nonfunctional forms (unfolded states, irreversibly-denatured protein)(Sanchez-Ruiz, 2010). Both the kinetic and thermodynamic stability of wild-type *Rho*1,2-CTD and each disulphide variant were determined and compared.

In terms of kinetic stability, two assays were performed, one to determine the temperature of half-inactivation (T_{50}) and the other to determine the half-life ($t_{1/2}$). T_{50} is used to quantify the loss of catalytic activity at higher temperatures, in particular representing the temperature at which the enzyme loses 50% of its activity after 15 min of incubation compared to a control. The two best-performing single disulphide variants K96C-D278C and A35C/Q211C displayed increases in half-inactivation (T_{50}) values of 4.6°C and 3.17°C respectively compared to the wild-type enzyme (Figure 3a,b; Table 1). Among the other variants, five (A44C/A44C, S116C-D181C, R95C-D278C, H85C-A252C, E231C-A280C) demonstrated an increase or decrease of less than 1°C, and two (K230C-A280C, V138C-A149C) demonstrated a decrease of more than 1°C. The double disulfide variants were only as good as the best single variants yielding 3.2°C and a 4.7°C increases in T_{50} for DB1 and DB2 respectively. To confirm these changes in kinetic stability, $t_{1/2}$ values were determined. This half-life value represents the amount of time it takes for the enzyme to lose 50% of its activity at a given temperature. The two best-performing single variants were K96C-D278C, consistent with T_{50}, and H85C-A252C which yielded 635% and 264% increases in $t_{1/2}$ at 40°C compared to the wild-type respectively (Figure 3c,d; Table 1). These values are reported in the context that while 40°C is the optimal temperature of the wild type enzyme. Other variants likely have different optimal temperatures. For example, we found that the optimal temperature of K96C-D278C was 45°C, and might have a different $t_{1/2}$ if assayed at this higher temperature. Among the other variants, two (R95C-D278C, A35C/Q211C) showed only small improvements, while five (S116C-D181C, E231C-A280C, K230C-A280C, A44C/A44C, V138C-A149C) showed decreases in $t_{1/2}$ compared to the wild-type. The two stacked disulfide yielded $t_{1/2}$ values somewhere between those arising from the single variants they were comprised of, at 501%, and 322% increases respectively for DB1 and DB2.

To determine thermodynamic stability, the melting temperature (T_m) of the enzymes was measured. T_m is a measure of structural stability and the protein unfolding process and represents the temperature at which 50% of the protein is unfolded. Overall, seven of the nine single disulfide variants and both stacked double disulfide variants displayed improved T_m over the wild type (Figure 3e,f; Table 1). Interestingly, the A35C/Q211C and DB1 (K96C-D278C + A35C/Q211C) showed the greatest increases, of more than 10°C in T_m compared to wild-type, consistent with their higher kinetic stability. Three other variants displayed increases of more than 5°C, including K96C-D278C (the best kinetic stabilized variant) as well as H85C-A252C, E231C-A280C. Three variants (A44C/A44C, R95C-D278C and V138C-A149C) displayed increases of between 1 and 3°C. Two variants (K230C-A280C, S116C-D181C) displayed decreases in Tm, consistent with their lower observed $t_{1/2}$ and T_{50} values.

3.4 | Catalytic activity and total turnover number of wild-type *Rho*1,2-CTD and disulphide variants

To determine the effect of the engineered disulphide variants on enzyme kinetics, Michaelis–Menten analyses of wild-type *Rho*1,2-CTD and its' disulphide variants were completed (Table 2; Supporting Information S1: Figure S6). Most of the variants had decreased catalytic efficiency compared to the wild-type enzyme. Of the variants that performed the best in terms of thermostability, K96C-D278C had a 28% decrease in catalytic efficiency and H85C-A252C had an 11% decrease. Thus, it was surprising that DB2 (K96C-D278C + H85C-A252C) had a substantial 40% increase in catalytic efficiency. Consideration of the contributing factors highlights that this increase is most likely attributable to increased productive substrate binding affinity, with DB2 yielding the lowest observed K_m value of any variant, 7.5-fold lower than wild type. This effect is consistent with the H85C-A252C bond being localized immediately adjacent to the catalytic pocket (Figure 2a), although the exact mechanism of increased affinity remains to be assessed. In this light it is also interesting to note that DB1 did not yield a comparable

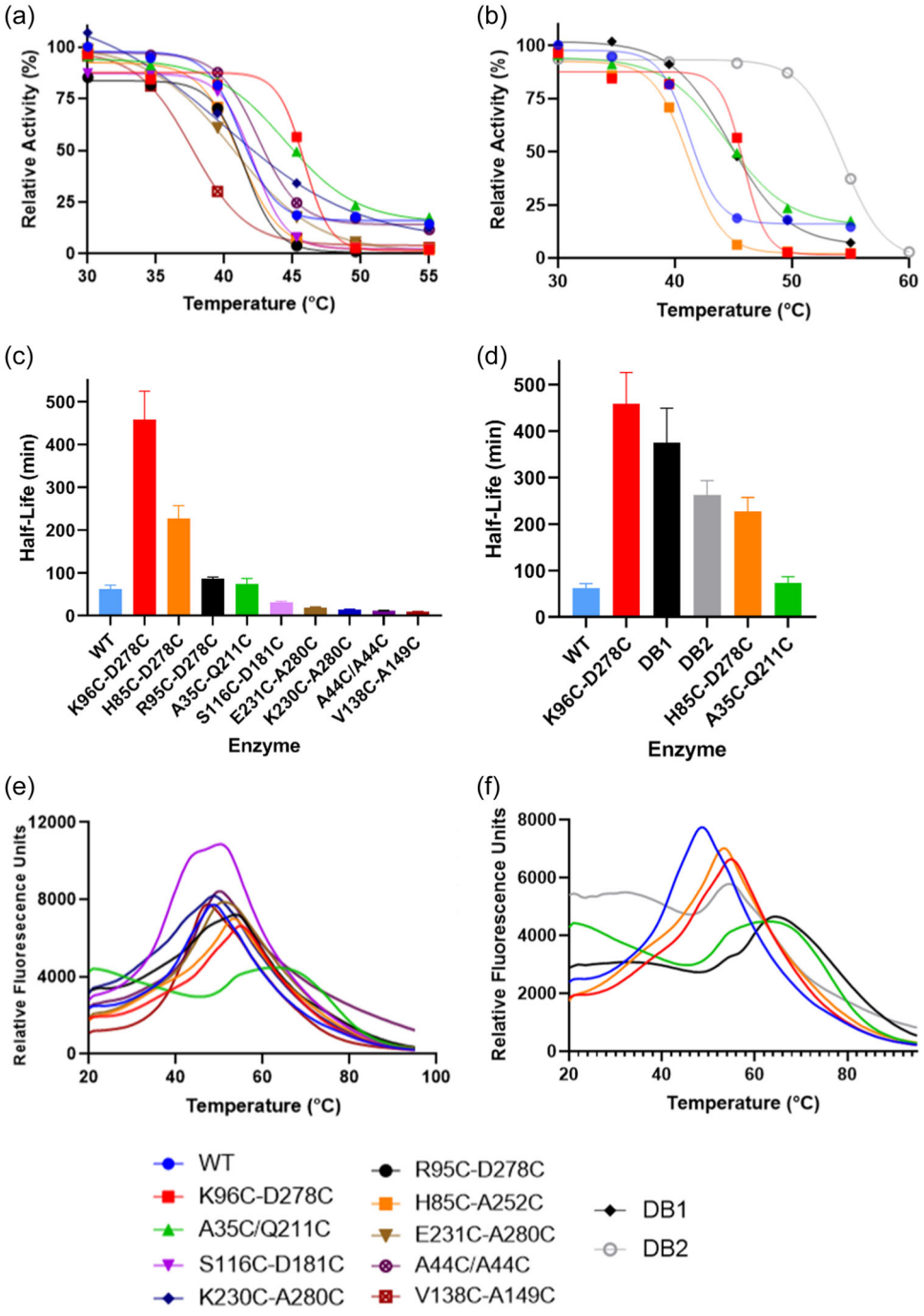

FIGURE 3 Thermostability analyses of wild type and variant *Rho*1,2-CTDs. T_{50} kinetic stability curves for single disulfide (a) and stacked double disulfide (b) variants. Enzymes were incubated for 15 min each at different temperatures and residual activity assayed at 25°C. Activity is reported as percentage of untreated enzyme activity at 25°C. Values are plotted along a Boltzmann sigmoidal curve and the value of T_{50} was obtained by determination of the inflection point of the curve. $t_{1/2}$ kinetic stability for single disulfide (c) and stacked double disulfide (d) variants. Enzymes were incubated at 40°C and residual activity assessed over time. The raw data were fit to first-order plots and analyzed with the first-order rate constants (k_d) determined by linear regression of ln(residual activity) versus incubation time. The half-life ($t_{1/2}$) represents the time required for the residual activity to be reduced to half, $t_{1/2} = \ln 2/k_d$. Values reported represent the mean of three technical replicates with error bars representing standard deviation. Tm thermodynamic stability curves for single disulfide (e) and stacked double disulfide (f) variants. Enzymes were incubated with SYPRO Orange dye and melting temperature by the increase in the raw fluorescence signal (shown) as the temperature increased. Tm represents the temperature where 50% of the protein is denatured and was determined at the temperature where dF/dT is at the global minimum. In all cases, values reported (Table 1) represent the mean of three technical replicates with error bars representing standard error.

increase in catalytic efficiency, despite A35C/Q211C having an 11% increase in k_{cat}, most likely attributable to the unexpected increase in K_m for DB1.

The continuous replacement of enzymes and other proteins appropriates up to half the maintenance energy budget in microorganisms and plants; thus, high enzyme replacement rates cut the productivity of biosystems (Hanson et al., 2021). Therefore, the expected product yield of a biocatalyst during its useful lifetime is an important consideration when designing biocatalytic processes (Rogers & Bommarius, 2010). One important indicator of lifetime biocatalyst productivity is the dimensionless total turnover number (TTN). The TTN of an enzyme represents the number of molecules of substrate converted to product by one molecule of enzyme before it's permanently deactivated. It can also be thought of as the number of catalytic cycles the enzyme performs before it denatures. In this study, an approximation was used to obtain the static TTN by dividing the value of k_{cat} by the enzyme deactivation constant k_d. Of the single disulfide variants, 4 had improved TTNs compared to wild type while 5 displayed decreases (Table 2). The best performing variant K96C-D278C demonstrated a >800% (9.4-fold) increase in TTN, driven by a 29% increase in k_{cat} and a sevenfold decrease in k_d relative to wild type. DB1 which also includes K96C-D278C showed only a 381% increase. The TTN of DB2, also including K96C-D278C, was virtually unchanged from that of wild type.

TABLE 1 Thermostability analysis of Rho1,2-CTD and disulphide variants.

Enzyme	Kinetic stability		Thermodynamic stability	
	T_{50} (°C)	$t_{1/2}$ (min)	T_m 1 (°C)	T_m 2 (°C)
Wild Type	41.1 ± 0.4	62.3 ± 9.4	41.8 ± 0.2	46.2 ± 0.2
K96C-D278C	45.9 ± 0.6	458 ± 66	47.3 ± 0.2	52.7 ± 0.2
DB 1	44.4 ± 0.7	375 ± 72	52.7 ± 0.2	59.5
DB 2	45.9 ± 0.8	263 ± 30	51.2 ± 0.2	
H85C-A252C	41.3 ± 0.5	227 ± 30	50.7 ± 0.2	
A35C/Q211C	44.7 ± 2.4	74 ± 12	52.3 ± 0.2	
R95C-D278C	41.9 ± 0.4	87.0 ± 3.4	44.0	
S116C-D181C	41.6 ± 0.1	31.5 ± 2.0	38.0	
E231C-A280C	39.4 ± 0.6	19.6 ± 1.3	47.0	
K230C-A280C	38[a]	14.4 ± 1.2	40.5	46.5
A44C/A44C	43 ± 1.4	12.0 ± 0.8	44.5	
V138C-A149C	37.5 ± 0.4	10.0 ± 0.4	43.7 ± 0.2	

[a]Note: data for mutant K230C-A280C should be interpreted with caution as this mutant did not fit the Boltzmann sigmoidal model used to obtain the T_{50}.

3.5 | Verification of disulfide bond formation

To verify the proper formation of disulfide bonds within the protein, the DTNB (5,5'-dithiobis-(2-nitrobenzoic acid) method was applied. In this method, DTNB reacts with free sulfhydryl groups in reduced and oxidized protein. The colored species 2-nitro-5-thiobenzoic acid is released and detected at 412 nm. Absorbance values are converted to free sulfhydryl concentration using a standard curve. Two free sulfhydryl groups were detected in each single disulfide variant tested under reducing conditions (Supporting Information S1: Figure S7). Four free sulfhydryl groups were detected in each double disulphide variant under reducing conditions. For K96C-D278C, H85C-A252C and DB2, there was <10% of the signal remaining under nonreducing

TABLE 2 Catalytic activity and total turnover data for the wild-type and disulfide variant Rho1,2-CTDs.

Variant	K_m (μM)	k_{cat} (min^{-1})	k_{cat}/K_m (min^{-1}• μM^{-1})	R^2 value	k_d (min^{-1})	TTN
Wild-Type	9 ± 2	157 ± 14	18 ± 5	0.8102	0.011 ± 0.002	14,164 ± 2491
K96C-D278C	16 ± 3	202 ± 5	13 ± 3	0.8124	0.0015 ± 0.0002	133,664 ± 19,518
R95C-D278C	49 ± 2	296 ± 20	6.0 ± 0.5	0.9197	0.0080 ± 0.0003	96,920 ± 11,905
DB #1	14 ± 3	126 ± 7	9 ± 2	0.8207	0.0019 ± 0.0004	68,216 ± 13,548
H85C-A252C	6.0 ± 0.5	97 ± 4	16 ± 2	0.8567	0.0030 ± 0.0004	36,766 ± 5773
S116C-D181C	23 ± 6	244 ± 43	10 ± 3	0.8974	0.022 ± 0.001	26,106 ± 6014
A35C/Q211C	5 ± 1	100 ± 5	21 ± 5	0.8129	0.0093 ± 0.002	12,597 ± 2527
DB #2	1.2 ± 0.5	30.2 ± 0.3	26 ± 12	0.5776	0.0026 ± 0.0003	11,440 ± 1330
E231C-A280C	12 ± 5	204 ± 19	16 ± 6	0.8584	0.035 ± 0.002	9726 ± 1315
A44C/A44C	27 ± 5	272 ± 25	10 ± 2	0.944	0.058 ± 0.004	5655 ± 703
K230C-A280C	6 ± 2	128 ± 13	21 ± 7	0.8029	0.048 ± 0.004	3621 ± 531
V138C-A149C	8 ± 2	101 ± 1	12 ± 3	0.8647	0.069 ± 0.003	1747 ± 79

conditions compared to reducing conditions, suggesting >90% of enzymes had properly formed disulfide bonds. For DB1 11% and for A35C/Q211C 19% of the signal was remaining under nonreducing conditions, suggesting that 89%, and 81% of enzymes had properly formed disulfide bonds respectively.

4 | DISCUSSION

The introduction of disulfide bonds into protein structure is a common strategy used to improve the thermostability of enzymes (Han et al., 2009; Hwa et al., 2014; Yin et al., 2015). However, if not done carefully, poorly-designed disulfide bonds can result in reduced catalytic activity, inferior thermostability and misfolding (Siadat et al., 2006; Wells & Powers, 1986; Wetzel et al., 1988). Therefore, a careful selection of residue pairs in the enzyme structure is required. In this study, 3 different software programs were applied to obtain a robust selection of possible designs. The outcome was a selection of variants, several with significantly improved stability compared to wild-type.

As mentioned previously, protein stability can be thermodynamic or kinetic (Sanchez-Ruiz, 2010). To gain a more complete overall picture of stability, both kinetic (T_{50}, $t_{1/2}$) and thermodynamic stability (Tm) were assessed. Notably, there was a substantial correlation between the T_{50} and $t_{1/2}$ results, with a Pearson r value of 0.75 and a one-tailed p-value of 0.0031, validating the kinetic stability outcomes. Overall, the variant K96C-D278C was shown to be the most stable with the greatest improvements in both T_{50} (4.7°C) and $t_{1/2}$ (635%) compared to wild-type. However, the second-best performing variant in each of these assays differed. A35C/Q211C had the second highest T_{50} (3.4°C) but only the fourth highest $t_{1/2}$ variant. On the other hand, H85C-A252C displayed the second highest $t_{1/2}$ (264%), but having no significant difference in T_{50} compared to wild-type. Factors potentially contributing to these variations are most likely related to the nature of the two kinetic stability assays. The T_{50} was obtained by heating to high temperatures for 15 min, followed by cooling to 25°C for measurement. In contrast, the $t_{1/2}$ was obtained by heating to 40°C for specific lengths of time and then measuring at 40°C. An enzyme with high T_{50} but low $t_{1/2}$, such as A35C/Q211C, could indicate that the enzyme unfolds at higher temperatures, but reversibly. Alternatively, an enzyme with high $t_{1/2}$ but low T_{50}, such as H85C-A252C could indicate that a first unfolding step is occurring, that lowers the activity of the enzyme, but does not lead to any other unfolding steps at the given temperature. In terms of thermodynamic stability, comparison of the T_m outcomes to the kinetic T_{50} and $t_{1/2}$ results shows only moderate correlation (Pearson $r = 0.60$, one-tailed p-value = 0.0191 for Tm and T_{50} and Pearson $r = 0.60$, one-tailed p-value = 47 for Tm and $t_{1/2}$). Nonetheless, the top performers for kinetic stability were also the best-performing in terms of thermodynamic stability (T_m) with K96C-D278C (5.5°C), H85C-A252C (8.8°C), and A35C/Q211C (10.5°C) all showing increases compared to wild-type. Interestingly, stacking of these top designs to make double disulfide variants did not yield any further significant gains.

Broadly, in the field of protein engineering, there is a well-known limitation referred to as the activity-stability trade-off (Tokuriki et al., 2008). This idea implies that an increase in activity is accompanied by a concomitant decrease in protein stability and vice versa. Therefore, it was important to test the kinetic parameters of the disulfide variants to determine the effect stabilization had on enzyme activity. Results from kinetic testing of the wild-type enzyme showed a similar K_m value to previously published results (K_m = 6.5 μM vs 9 μM). However, the k_{cat} obtained herein was smaller than that previously obtained (k_{cat} = 636.9 min^{-1} vs 157 min^{-1}) (Matera et al., 2010). This difference is most likely arising due to the enzyme used in this study being produced recombinantly and containing a His-tag, while in the other study the enzyme was obtained from the native source (Matera et al., 2010). Previous studies have correlated the presence of His-tags with decreased catalytic activity (Meng et al., 2020). With respect to kinetics of the most highly stabilized variants, K96C-D278C and H85C-A252C showed substantial decreases in catalytic efficiency of 37%, and 21% respectively compared to wild type, while A35C/Q211C had little effect (Table 2). While it would be ideal to suffer no loss in catalytic activity, as of the time of writing, we could not find in the literature any example of an engineered enzyme design that was able to overcome this trade-off. Nevertheless, the loss of catalytic activity in some of these disulfide variants are relatively minor, notably when taken in comparison to the relative increases in stability.

To furthermore obtain a sense of the balance between activity and stability, and the overall utility of the stabilized variants, the static total turnover number (TTN) was calculated. The TTN represents total number of substrates reacted per enzyme, where its calculation is an approximation obtained by dividing the turnover number (k_{cat}) by the deactivation constant, k_d (obtained from $t_{1/2}$ testing). Hence the value of TTN is dependent on a combination of activity and stability, such that a higher TTN is interpreted to mean a higher combined activity and stability. In this measure, once again the variant K96C-D278C stands above the rest, with over a 10-fold increase in TTN compared to the wild-type, with the bulk of the effect arising from a significant decrease in k_d (Table 1).

Another recurring theme, noted in disulfide engineering experiments, is the observation that engineered disulfide bonds linking regions of relatively high mobility are those most likely to confer stability to the protein (Clarke & Fersht, 1993; Dombkowski et al., 2014; Eijsink et al., 2001; Wedemeyer et al., 2000). This idea appears to originate from an analysis of previously engineered disulfide bonds where the effect on protein stability had been characterized and published (Matsumura et al., 1989). In this analysis, the authors investigated the relationship between several structural features of each disulfide bond and the change in stability. In summary, they reported: (1) stabilizing mutations were most often found in regions of medium to high mobility; (2) stabilizing mutations

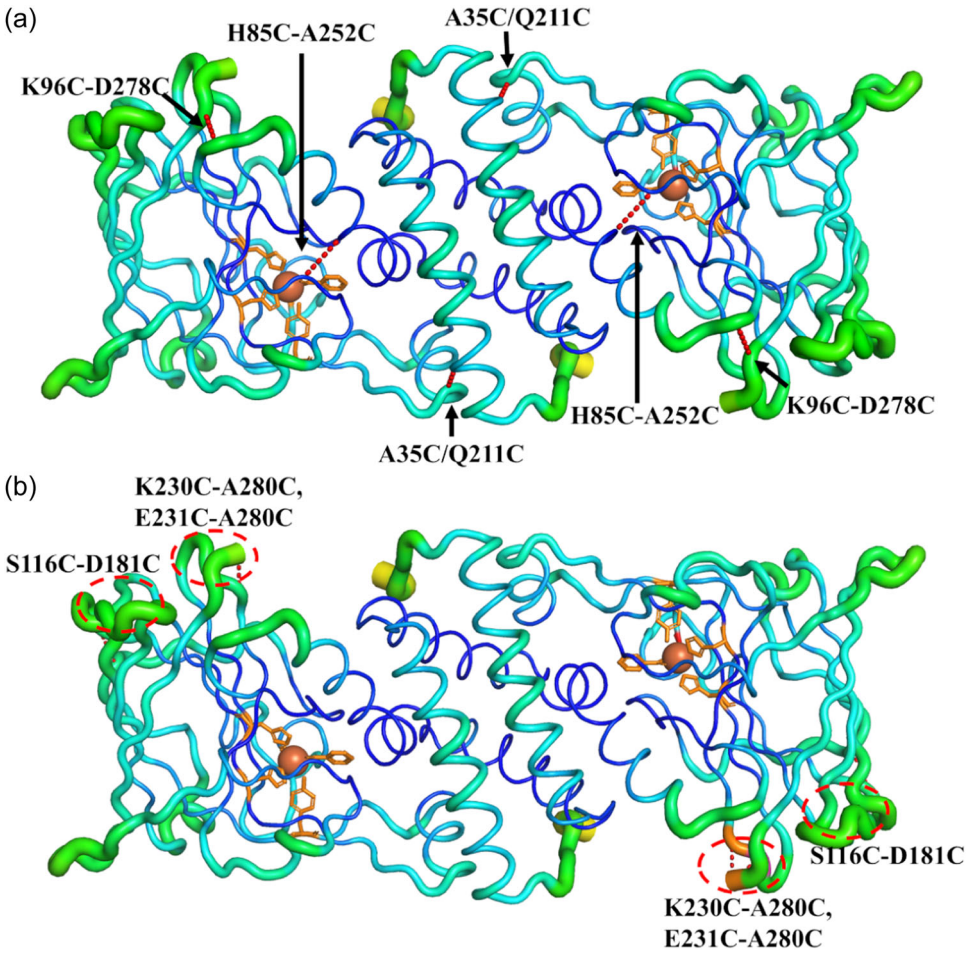

FIGURE 4 B-factor putty representation of *Rho*1,2-CTD (PDB ID: 3HGI) biological assembly showcasing locations of (a) top-performing and (b) lesser-performing disulfide bonds. The image was generated using the B-factor putty view function on PyMol. The backbone of the structure is displayed as a tube with a diameter and colour scheme correlated to the B-factor of the structure. Orange to red colours and a wider tube indicate regions with higher B-factors, whereas shades of blue and a narrower tube indicate regions with lower B-factors. Red dashed circles indicate the general location of disulphides that are hidden in the representation.

were more likely to be near the protein surface; (3) stabilizing mutations were associated with longer loop lengths (>25 residues); and (4) the introduced disulfide bond should not cause steric overlap.

Comparison of the best-performing disulfide designs herein to these criteria yields a mixed outcome. The overall best-performing single disulfide mutant K96C-D278C, is located near the C-terminus (Figure 2). Both cysteine residues forming this bond are in highly flexible loop regions of the protein Cα chain, as quantified by their B-factors in the structure file (Figure 4a). This bond is also located close to the protein surface and has a large loop length enclosed by the disulfide. It also does not cause steric overlap. Similarly, for A35C/Q211C, one of the next two best-performing variants, the disulphide connects the two monomers of the *Rho*1,2-CTD homodimer. Disulfide bonds can play important roles in stabilizing protein quaternary structures (Wedemeyer et al., 2000), such that stabilization of the dimer might be expected to increase stability. In terms of flexibility, the residue Q211 is in a highly flexible loop region of the protein while residue A35 is in a helical region of moderate flexibility (Figure 4a). This bond is also located close to the protein surface, has a large loop length enclosed by the disulfide, and does not cause steric overlap. Thus, overall, both of these top design hits fit well with the criteria listed above (Matsumura et al., 1989) and summarized previously (Dani et al., 2003).

The final top performing design, H85C-A252C, connects the catalytic and dimerization domains of *Rho*1,2-CTD. Interestingly, and in contrast, this design does not fit all of the four disulfide criteria defined above and previously (Dani et al., 2003). While it does have a large loop length enclosed by the disulfide, and does not cause steric overlap, it is located within the core of the protein and in a region with low relative flexibility. In fact, as mentioned in the methods section, this bond did not actually pass step 3 in the design pipeline (Supporting Information S1: Figure S2) with both residues being among the 25% least flexible residues of *Rho*1,2-CTD based on their crystallographic B-factors (Figure 4a). An exception was made to include this design as

this bond is located at a domain interface and was predicted to be strongly stabilizing in step 4 of the design pipeline (Supporting Information S1: Figure S2; by the program DynaMut2 (Rodrigues et al., 2021)). This outcome highlights the relevance of domain-domain interactions in overall stability and may be relevant to stability as a region of the protein that unfolds first (Clarke & Fersht, 1993; Mansfeld et al., 1997). On the other hand, Additionally, this mutant performed considerably better than the many other designs tested, which were located in regions of higher flexibility. Take for example the K230C-A280C, E231C-A280C, and S116C-D181C designs, which were among the worst performing (Table 1). Yet all of these residues were located in highly flexible regions of the protein (Figure 4b). Thus, while a limited sample, the findings herein suggest that although targeting of flexible regions can be effective, it is not always prescriptive, and modulation of factors other than flexibility can be leveraged to impart higher stability as well.

Overall, multiple thermostable *Rho*1,2-CTD variants were engineered via the introduction of disulfide bonds. These disulfide variants were designed using disulfide bond prediction software programs combined with a novel selective design pipeline. Several variants displayed significantly improved thermostability properties. Whether any significant design hits were eliminated during the selection goes beyond the scope of this current study, but remains an interesting question for future consideration. In conclusion, current state-of-the-art disulfide bond prediction algorithms can be highly effective for designing improved protein thermostability into biocatalysts. At the same time, the potential to stabilize members of the intradiol ring-cleaving family of enzymes is emphasized.

AUTHOR CONTRIBUTIONS

Joshua G.R. Lister carried out all of the experiments and analyzed and interpreted all the data and wrote the first draft of the paper. Matthew E. Loewen conceived of some of the ideas, obtained funding, and helped write the paper. Michele C. Loewen conceived of some ideas, obtained funding, oversaw planning and data interpretation and finalized writing the manuscript. Antony D. St-Jacques conceived of some ideas, planned most experiments, trained Joshua G.R. Lister in all experimental aspects, interpreted data and edited the paper.

ACKNOWLEDGMENTS

This work was funded by an Alliance Grant from the Natural Sciences and Engineering Research Council held by both Michele C. Loewen and Matthew E. Loewen (#550057 – 20) and by the National Research Council of Canada to Michele C. Loewen. This report represents National Research Council of Canada Communication # 58482. This project was funded by the Natural Sciences and Engineering Research Council – Alliance Program [Project # ALLRP 550057-20] to Matthew E. Loewen and Michele C. Loewen. Open Access funding provided by the National Research Council Canada library.

DATA AVAILABILITY STATEMENT

The data that support the findings of this study are available from the corresponding author upon reasonable request.

ORCID

Michele C. Loewen http://orcid.org/0000-0001-5053-9512
Antony D. St-Jacques https://orcid.org/0000-0002-6194-6890

REFERENCES

Abkevich, V. I., & Shakhnovich, E. I. (2000). What can disulfide bonds tell us about protein energetics, function and folding: Simulations and bioninformatics analysis. *Journal of Molecular Biology*, *300*(4), 975–985. https://doi.org/10.1006/jmbi.2000.3893

Badieyan, S., Bevan, D. R., & Zhang, C. (2012). Study and design of stability in GH5 cellulases. *Biotechnology and Bioengineering*, *109*(1), 31–44. https://doi.org/10.1002/bit.23280

Betz, S. F. (1993). Disulfide bonds and the stability of globular proteins. *Protein Science*, *2*(10), 1551–1558. https://doi.org/10.1002/pro.5560021002

Bradford, M. M. (1976). A rapid and sensitive method for the quantitation of microgram quantities of protein utilizing the principle of protein-dye binding. *Analytical Biochemistry*, *72*(1–2), 248–254. https://doi.org/10.1016/0003-2697(76)90527-3

Bugg, T. D., & Ramaswamy, S. (2008). Non-heme iron-dependent dioxygenases: Unravelling catalytic mechanisms for complex enzymatic oxidations. *Current Opinion in Chemical Biology*, *12*(2), 134–140. https://doi.org/10.1016/j.cbpa.2007.12.007

Bugg, T. D. H., & Lin, G. (2001). Solving the riddle of the intradiol and extradiol catechol dioxygenases: How do enzymes control hydroperoxide rearrangements?*In Chemical Communications* (pp. 941–952). Royal Society of Chemistry. https://doi.org/10.1039/b100484k

Clarke, J., & Fersht, A. R. (1993). Engineered disulfide bonds as probes of the folding pathway of barnase: Increasing the stability of proteins against the rate of denaturation. *Biochemistry*, *32*(16), 4322–4329. https://doi.org/10.1021/bi00067a022

Craig, D. B., & Dombkowski, A. A. (2013). Disulfide by design 2.0: A web-based tool for disulfide engineering in proteins. *BMC Bioinformatics*, *14*(1), 346. https://doi.org/10.1186/1471-2105-14-346

Dani, V. S., Ramakrishnan, C., & Varadarajan, R. (2003). MODIP revisited: Re-evaluation and refinement of an automated procedure for modeling of disulfide bonds in proteins. *Protein Engineering, Design and Selection*, *16*(3), 187–193. https://doi.org/10.1093/proeng/gzg024

Dombkowski, A. A., Sultana, K. Z., & Craig, D. B. (2014). Protein disulfide engineering. *FEBS Letters*, *588*(2), 206–212. https://doi.org/10.1016/j.febslet.2013.11.024

Eijsink, V. G. H., Vriend, G., & Van Den Burg, B. (2001). Engineering a hyperstable enzyme by manipulation of early steps in the unfolding process. *Biocatalysis and Biotransformation*, *19*(5–6), 443–458. https://doi.org/10.3109/10242420108992029

Ellman, G. L. (1959). Tissue sulfhydryl groups. *Archives of Biochemistry and Biophysics*, *82*(1), 70–77. https://doi.org/10.1016/0003-9861(59)90090-6

Environment and Climate Change Canada. (2023). *Canadian environmental sustainability indicators: Greenhouse gas emissions*. Environment and Climate Change Canada.

Forero, N., Liu, C., Sabbah, S. G., Loewen, M. C., & Yang, T. C. (2023). Assay development for metal-dependent enzymes—influence of reaction buffers on activities and kinetic characteristics. *ACS Omega*, *8*, 40119–40127. https://doi.org/10.1021/acsomega.3c02835

Gao, X., Dong, X., Li, X., Liu, Z., & Liu, H. (2020). Prediction of disulfide bond engineering sites using a machine learning method. *Scientific Reports*, *10*(1), 10330. https://doi.org/10.1038/s41598-020-67230-z

Han, Z., Han, S., Zheng, S., & Lin, Y. (2009). Enhancing thermostability of a *Rhizomucor miehei* lipase by engineering a disulfide bond and displaying on the yeast cell surface. *Applied Microbiology and*

Biotechnology, *85*(1), 117–126. https://doi.org/10.1007/s00253-009-2067-8

Hanson, A. D., McCarty, D. R., Henry, C. S., Xian, X., Joshi, J., Patterson, J. A., García-García, J. D., Fleischmann, S. D., Tivendale, N. D., & Millar, A. H. (2021). The number of catalytic cycles in an enzyme's lifetime and why it matters to metabolic engineering. *Proceedings of the National Academy of Sciences*, *118*(13), e2023348118. https://doi.org/10.1073/pnas.2023348118/-/DCSupplemental

Hogg, P. J. (2003). Disulfide bonds as switches for protein function. *Trends in Biochemical Sciences*, *28*(4), 210–214. https://doi.org/10.1016/S0968-0004(03)00057-4

Hwa, K.-Y., Subramani, B., Shen, S.-T., & Lee, Y.-M. (2014). An intermolecular disulfide bond is required for thermostability and thermoactivity of β-glycosidase from Thermococcus kodakarensis KOD1. *Applied Microbiology and Biotechnology*, *98*(18), 7825–7836. https://doi.org/10.1007/s00253-014-5731-6

Karimi, M., Ignasiak, M. T., Chan, B., Croft, A. K., Radom, L., Schiesser, C. H., Pattison, D. I., & Davies, M. J. (2016). Reactivity of disulfide bonds is markedly affected by structure and environment: Implications for protein modification and stability. *Scientific Reports*, *6*(1), 38572. https://doi.org/10.1038/srep38572

Kazlauskas, R. (2018). Engineering more stable proteins. *Chemical Society Reviews*, *47*(24), 9026–9045. https://doi.org/10.1039/C8CS00014J

Landeta, C., Boyd, D., & Beckwith, J. (2018). Disulfide bond formation in prokaryotes. *Nature Microbiology*, *3*(3), 270–280. https://doi.org/10.1038/s41564-017-0106-2

Liu, L., Deng, Z., Yang, H., Li, J., Shin, H., Chen, R. R., Du, G., & Chen, J. (2014). In silico rational design and systems engineering of disulfide bridges in the catalytic domain of an alkaline α-amylase from *Alkalimonas amylolytica* to improve thermostability. *Applied and Environmental Microbiology*, *80*(3), 798–807. https://doi.org/10.1128/AEM.03045-13

Mansfeld, J., Vriend, G., Dijkstra, B. W., Rob Veltman, O., Van den Burg, B., Venema, G., Ulbrich-Hofmann, R., & H.Eijsink, V. G. (1997). Extreme Stabilization of a Thermolysin-like Protease by an Engineered Disulfide Bond. *Journal of Biological Chemistry*, *272*(17), 11152–11156. https://doi.org/10.1074/jbc.272.17.11152

Matera, I., Ferraroni, M., Kolomytseva, M., Golovleva, L., Scozzafava, A., & Briganti, F. (2010). Catechol 1,2-dioxygenase from the gram-positive *Rhodococcus opacus* 1CP: Quantitative structure/activity relationship and the crystal structures of native enzyme and catechols adducts. *Journal of Structural Biology*, *170*(3), 548–564. https://doi.org/10.1016/J.JSB.2009.12.023

Matsumura, M., Becktel, W. J., Levitt, M., & Matthews, B. W. (1989). Stabilization of phage T4 lysozyme by engineered disulfide bonds. *Proceedings of the National Academy of Sciences*, *86*, 6562–6566.

Meng, L., Liu, Y., Yin, X., Zhou, H., Wu, J., Wu, M., & Yang, L. (2020). Effects of His-tag on catalytic activity and enantioselectivity of recombinant transaminases. *Applied Biochemistry and Biotechnology*, *190*(3), 880–895. https://doi.org/10.1007/s12010-019-03117-8

Michaelis, L., & Menten, M. L. (1913). Die kinetik der invertinwirkung. *Biochemische Zeitschrift*, *49*, 333–369. http://publikationen.ub.uni-frankfurt.de/frontdoor/index/index/docId/17273

Niesen, F. H., Berglund, H., & Vedadi, M. (2007). The use of differential scanning fluorimetry to detect ligand interactions that promote protein stability. *Nature Protocols*, *2*(9), 2212–2221. https://doi.org/10.1038/nprot.2007.321

Pace, C. N., Grimsley, G. R., Thomson, J. A., & Barnett, B. J. (1988). Conformational stability and activity of ribonuclease T1 with zero, one, and two intact disulfide bonds. *Journal of Biological Chemistry*, *263*(24), 11820–11825. https://doi.org/10.1016/S0021-9258(18)37859-1

Petersen, M. T. N., Jonson, P. H., & Petersen, S. B. (1999). Amino acid neighbours and detailed conformational analysis of cysteines in proteins. *Protein Engineering, Design and Selection*, *12*(7), 535–548. https://doi.org/10.1093/protein/12.7.535

PyMOL. (2024). The PyMOL Molecular Graphics System, Version 3.0 Schrödinger, LLC. In Available from http://www.pymol.org/pymol

Que, L., & Ho, R. Y. N. (1996). Dioxygen activation by enzymes with mononuclear non-heme iron active sites. *Chemical Reviews*, *96*(7), 2607–2624. https://doi.org/10.1021/cr960039f

Rodrigues, C. H. M., Pires, D. E. V., & Ascher, D. B. (2021). DynaMut2: Assessing changes in stability and flexibility upon single and multiple point missense mutations. *Protein Science*, *30*(1), 60–69. https://doi.org/10.1002/pro.3942

Roesler, K. R., & Rao, A. G. (2000). A single disulfide bond restores thermodynamic and proteolytic stability to an extensively mutated protein. *Protein Science*, *9*(9), 1642–1650. https://doi.org/10.1110/ps.9.9.1642

Rogers, T. A., & Bommarius, A. S. (2010). Utilizing simple biochemical measurements to predict lifetime output of biocatalysts in continuous isothermal processes. *Chemical Engineering Science*, *65*(6), 2118–2124. https://doi.org/10.1016/j.ces.2009.12.005

Rorrer, N. A., Dorgan, J. R., Vardon, D. R., Martinez, C. R., Yang, Y., & Beckham, G. T. (2016). Renewable unsaturated polyesters from muconic acid. *ACS Sustainable Chemistry & Engineering*, *4*(12), 6867–6876. https://doi.org/10.1021/acssuschemeng.6b01820

Rosa, N., Ristic, M., Seabrook, S. A., Lovell, D., Lucent, D., & Newman, J. (2015). Meltdown: A tool to help in the interpretation of thermal melt curves acquired by differential scanning fluorimetry. *SLAS Discovery*, *20*(7), 898–905. https://doi.org/10.1177/1087057115584059

Sanchez-Ruiz, J. M. (2010). Protein kinetic stability. *Biophysical Chemistry*, *148*(1), 1–15. https://doi.org/10.1016/j.bpc.2010.02.004

Shumkova, E. S., Solyanikova, I. P., Plotnikova, E. G., & Golovleva, L. A. (2009). Phenol degradation by *Rhodococcus opacus* strain 1G. *Applied Biochemistry and Microbiology*, *45*(1), 43–49. https://doi.org/10.1134/S0003683809010086

Siadat, O. R., Lougarre, A., Lamouroux, L., Ladurantie, C., & Fournier, D. (2006). The effect of engineered disulfide bonds on the stability of *Drosophila melanogaster* acetylcholinesterase. *BMC Biochemistry*, *7*(1), 12. https://doi.org/10.1186/1471-2091-7-12

Suplatov, D., Timonina, D., Sharapova, Y., & Švedas, V. (2019). Yosshi: A web-server for disulfide engineering by bioinformatic analysis of diverse protein families. *Nucleic Acids Research*, *47*(W1), W308–W314. https://doi.org/10.1093/nar/gkz385

Thiemens, M. H., & Trogler, W. C. (1991). Nylon production: An unknown source of atmospheric nitrous oxide. *Science*, *251*, 932–934. https://www.science.org

Tokuriki, N., Stricher, F., Serrano, L., & Tawfik, D. S. (2008). How protein stability and new functions trade off. *PLoS Computational Biology*, *4*(2), e1000002. https://doi.org/10.1371/journal.pcbi.1000002

Wedemeyer, W. J., Welker, E., Narayan, M., & Scheraga, H. A. (2000). Disulfide bonds and protein folding. *Biochemistry*, *39*(15), 4207–4216. https://doi.org/10.1021/bi992922o

Wells, J. A., & Powers, D. B. (1986). In vivo formation and stability of engineered disulfide bonds in subtilisin. *Journal of Biological Chemistry*, *261*(14), 6564–6570. https://doi.org/10.1016/S0021-9258(19)84599-4

Wetzel, R., Perry, L. J., Baase, W. A., & Becktel, W. J. (1988). Disulfide bonds and thermal stability in T4 lysozyme. *Proceedings of the National Academy of Sciences*, *85*(2), 401–405. https://doi.org/10.1073/pnas.85.2.401

Xie, N.-Z., Liang, H., Huang, R.-B., & Xu, P. (2014). Biotechnological production of muconic acid: Current status and future prospects.

Biotechnology Advances, *32*(3), 615–622. https://doi.org/10.1016/j.biotechadv.2014.04.001

Xie, Y., An, J., Yang, G., Wu, G., Zhang, Y., Cui, L., & Feng, Y. (2014). Enhanced enzyme kinetic stability by increasing rigidity within the active site. *Journal of Biological Chemistry*, *289*(11), 7994–8006. https://doi.org/10.1074/jbc.M113.536045

Yin, X., Hu, D., Li, J.-F., He, Y., Zhu, T.-D., & Wu, M.-C. (2015). Contribution of disulfide bridges to the thermostability of a type A feruloyl esterase from *Aspergillus usamii*. *PLoS One*, *10*(5), e0126864. https://doi.org/10.1371/journal.pone.0126864

Zhang, L., Chou, C. P., & Moo-Young, M. (2011). Disulfide bond formation and its impact on the biological activity and stability of recombinant therapeutic proteins produced by *Escherichia coli* expression system. *Biotechnology Advances*, *29*(6), 923–929. https://doi.org/10.1016/j.biotechadv.2011.07.013

SUPPORTING INFORMATION

Additional supporting information can be found online in the Supporting Information section at the end of this article.

How to cite this article: Lister, J. G. R., Loewen, M. E., Loewen, M. C., & St-Jacques, A. D. (2024). Rational design of disulfide bonds to increase thermostability of *Rhodococcus opacus* catechol 1,2 dioxygenase. *Biotechnology and Bioengineering*, 1–13. https://doi.org/10.1002/bit.28808